Development of a novel combined fluorescence and reflectance spectroscopy system for guiding high-grade glioma resections

Monirehalsadat Mousavi

Master's Thesis
LRAP-476
2013

Lund University

Abstract

Total resection of glioblastoma multiform (GBM), the most common and aggressive malignant brain tumor, continues to be a challenge. Achieving complete resection is limited by difficulty in intraoperative discrimination between normal and residual tumor cells. This project contributes to the development and evaluation of a fiber-optical based fluorescence/reflectance spectroscopy system as an intraoperative guiding tool, using δ-aminolevulinic acid (ALA)-induced Protoporphyrin IX (PpIX). The main aim is to combine the diagnostic potential of reflectance and fluorescence to improve clinical applicability. In this context, 5 LEDs coupled to a hand-held optical fiber was employed to deliver UV/visible light to the sample sequentially. Remitted light from the tissue; including diffuse reflected and fluorescence of endogenous and exogenous fluorophores, as well as its photobleaching product, is transmitted to one photodiode and four avalanche photodiodes. This instrument has been evaluated with very promising results by performing various tissue-equivalent phantom laboratory and clinical studies.

POPULAR SCIENCE

A primary brain tumor is an abnormal growth of cells in brain tissue. Brain tumors are classified as either benign (not invading healthy tissue) or malignant (infiltrating and destroying healthy tissue), depending on their degree of malignancy and aggressiveness. Benign brain tumors grow slowly and will not invade and destroy surrounding tissue, but will grow as a solid encapsulated tumor. Benign tumors thus have a clear border and can be removed. Malignant brain tumors contain cancer cells, are usually rapidly growing and life-threatening. These tumors intend to spread into the nearby healthy brain tissue and may recur after treatment. Glioblastoma multiform (GBM) is an example of highly malignant brain tumors. The prognosis for patients with GBM is of high concern, as it is associated with fast growth. Without therapy, patients die within three months and with optimal therapy, have a mean survival of approximately 12 months [1]. The main challenge in the therapy of this tumor is associated with its infiltrative growth and visual similarity of GBM to the surrounding brain tissue so that complete resection under white light, even in experienced hands, is between 13% and 20% [2].

Among all technologies and treatment algorithms employed in the treatment of this tumor type, intraoperative fluorescent tumor visualization has shown great promise. In this study, we aimed at developing a combined fluorescence/reflectance spectroscopy system that can assist the surgeon in distinguishing tissue types during brain tumor resection. The contrast agent used to provide the fluorescence contrast is δ-aminolevulinic acid (ALA)-induced protoporphyrin IX (PpIX). The ALA is administered orally to the patient prior to surgery. Malignant glial tumor tissue will then build up a higher concentration of Protoporphyrin IX, providing a fluorescence peak at 635 nm following 405 nm light excitation. The primary goal is obviously to provide a signal with high sensitivity and specificity for malignant tissue. Successful performance evaluation of this instrument has been demonstrated by performing various tissue-equivalent phantom laboratory and clinical studies.

ACRONYMS AND ABBREVIATIONS

ALA	δ-aminolevulinic acid
PpIX	Protoporphyrin IX
OTP	Optical Touch Pointer
CNS	Central Nervous System
GBM	Glioblastoma Multiform
CT	Computed Tomography
MRI	Magnetic Resonance Imaging
FGR	Fluorescence Guided Resection
iMRI	Intraoperative Magnetic Resonance Imaging
BBB	Blood-brain Barrier
IR	Infrared
NIR	Near-infrared
NADH	Nicotinamide adenine dinucleotide
FAD	Flavin adenine dinucleotide
PDT	Photodynamic Therapy
PCA	Principal Components Analysis
CA	Correspondence Analysis
MDS	Multidimensional Scaling
PLS	Partial Least Square
PCR	Principal Component Regression
MLVR	Multiple Linear Regression Analysis
LOOCV	Leave-one-out cross-validation
LED	Light-emitting diode
DAQ	Data acquisition
APD	Avalanche photodiodes

PD	Photodiode
FFT	Fast Fourier Transfer
DCM	4-(dicyanomethylene)-2-methyl-6-(p-dimethylaminostyryl)-4H-pyran
APD	Avalanche photodiodes
PD	Photodiode

Contents

Chapter 1

Introduction

Surgical resection of glioblastoma tumors, the most common and aggressive type of malignant brain tumor, is difficult due to its similarity in appearance to surrounding brain tissue and its infiltrative growth pattern. The standard method used today for tissue discrimination during surgical resections is visual inspection and palpation. Ultrasound and MR images are also taken before and after surgery in order to locate the tumor, delineate the borders between malignant and healthy tissue, as well as to verify the result of the resection. This information is not always sufficient for optimal surgical results.

The main idea of this project is to develop a system that can assist the surgeon in distinguishing tissue types during brain tumor resection. This system is based on an optical fiber probe, enabling *in vivo* fluorescence and reflectance spectroscopy during surgery. The tissue discrimination in the fluorescence signals is based on both endogenous fluorescence and contrast agents, while the reflectance correlates with optical properties of the tissue. The contrast agent employed is δ-aminolevulinic acid (ALA)-induced protoporphyrin IX (PpIX). It is assumed that the PpIX concentration is well correlated with the malignant transformation of the tissue. The ALA is administered orally to the patient prior to surgery. Malignant glial tumor tissue will then build up a higher concentration of Protoporphyrin IX, providing a fluorescence peak at 635 nm following 405 nm light excitation. The primary goal is obviously to provide a signal with high sensitivity and specificity for malignant tissue.

The idea for the system is thus to combine multi-wavelength diffuse reflection and fluorescence signals to obtain information related to PpIX concentration, independent on the amount of blood in the tissue. This would be an improvement to the the previous generation of this setup, called optical touch pointer (OTP) [3], which was also somewhat sensitive to ambient light during the

measurements, such as microscope lamp and room light in the operating room. In that system laser was as a source for fluorescence excitation illumination and a spectrometry method was used to detect fluorescence signals during tumor resection. The suppression capability of background light was not fully optimal, mainly due to that the signal integration time was rather long. In this study, by pulsing the light sources and employing lock-in type detection, this ambient light can very efficiently be suppressed in the detection. This method has in lab tests proven to detect very low PpIX fluorescence concentrations in tissue phantoms, with insignificant influence of ambient light. An *in vivo* elaborate test on skin tumor was conducted with this specific system to demonstrate its full capability, before the systems will be taken into use in the ongoing clinical research program for glioblastoma tumors conducted in collaboration with Linköping University.

Chapter 2 contains a general description of the anatomy of human brain and brain tumors, concludes with a subsection focusing on the surgical diagnosis and resection of brain tumors modalities. Chapter 3 contains a general introduction to the concept of light propagation through the biological tissue. Chapter 4 describes the design of the instrument and the analysis methodology, as well as the samples contents. The following chapters provide the results, describing the experimental procedures using a phantom that mimics the brain optical properties and the *in vivo* clinical trials. An overview of the main findings of this study and evaluation of the current state of project as well as future work of this project are included in chapter 7.

Chapter 2

Brain

2.1 The Human Brain

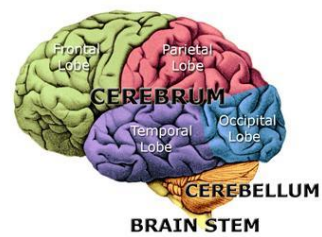

Figure 2.1. *Anatomy of the brain.(Image adapted from [4]).*

The human central nervous system (CNS) is part of neural tissue which is encapsulated within the skull and spinal cord and localized in the brain and spinal cord. The brain, the most complex organ of body, constitutes 2% of the body weight, while it consumes more than 30% of its energy supply. The major region of the brain includes the cerebrum, cerebellum and brainstem, see Fig. 2.1. The cerebrum contains the largest compartment of brain. It can be divided in the left and right cerebral hemispheres, each composed of outer gray matter (2 to 4mm) [6] and white matter (the bulk of the brain), see Fig. 2.2. Gray matter is also called cerebral cortex and comprises neurons, or nerve cell bodies and their dendrites as well as glial cells. The inner white matter consists mostly of glial cells and nerve fibers. The cerebrum is associated with several body functions, some of which include thinking, perceiving, movement, parts of speech, planning and organization. The cerebellum can in a similar way be divided in left and right cerebellar hemispheres and the vermis in between these two parts. The cerebellum is involved in the regulation and coordination of muscle activity. The brainstem, located between the cerebrum and the spinal cord, comprises the midbrain, the pron and the medulla. This structure is responsible for various vital functions such as regulating the respiratory and cardiac systems, as well as auditory and visual reflexes, etc. [7].

The nervous system is built from billions of cells, mainly neurons and glial cells [8]. Glial cells occupy half of the brain and support and protect the neurons and also supply nutrients and oxygen to the neurons. Nerve fibers, mainly located in the white matter are involved in transmitting signals to and from the brain.

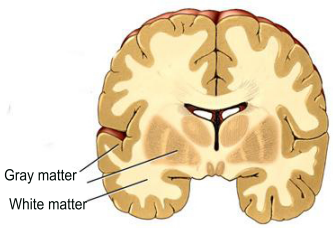

Figure 2.2. *Frontal section of brain.(Image adapted from [5]).*

2.2 Brain Tumors

A brain tumor is referred to as an unnecessary growing of cells in the brain. There are two types of brain tumors, primary brain tumors and metastatic brain tumors. The former includes any tumor that originates and tends to stay in the brain, while the latter is a malignant lesion originating in any part of the body and is spread to the brain. Brain tumors are classified depending on the region of the tumor, the type of tissue involved, whether they are benign or malignant and also how they appear under the microscope. Tumors are diagnosed, named and graded based on their classification system. This grading and classification system facilitates the planning of the treatment and the prediction of the outcome [9]. The grade of tumor indicates its level of malignancy.

Grade I tumors, according to the WHO grading system, are the least malignant and slow growing brain tumors. A grade I tumor, which is often considered as benign, occurs more frequently in children and is associated with long-term survival. It has a normal appearance under the microscope and surgery is often a sufficient treatment for these tumors.

Grade II is more common between the age of 20-50. Such tumors are relatively slow growing and the cells look slightly abnormal in the microscope. Recurrence sometimes happens even after complete surgical removal. Patients with such a tumor need to be followed up after surgery to detect any recurrence at an early stage, and may be considered for additional treatment options.

Grade III indicates a high grade tumor. Such a tumor actively reproduces abnormal cells. Such tumors tend to spread to nearby normal tissue of the brain and often recur after treatment as a higher grade of tumor.

Grade IV is a highly malignant brain tumor. A grade IV brain tumor grows fast and forms new blood vessels, so as to maintain its rapid growth. Glioblastoma is the most common example of this grade of tumor.

The most common type of brain tumor is glioma which arises from glial cells and counting 30% of the brain malignancies [10]. Gliomas, as these tumors are called, have a variety of grades and are divided to three main types: astrocytoma, oligodendroglioma, and mixed oligoastrocytomas [11].

Astrocytoma tumors are the most common type of glioma and can be divided into two categories: 1) protoplasmic astrocytes are typically found in gray matter and 2) fibrillary astrocytes (glioblastoma) usually located within white matter.

These tumors range from low grade to highly malignant. A low grade astrocytoma can be removed completely by surgery and many patients live for long periods of time after diagnosis. It is believed that this type of tumor in adults has the potential to recur, manifesting as higher grade tumors. The highest graded astrocytoma is grade IV glioblastoma (grade IV GBM) and accounts for approximately 50% of Astrocytomas tumors.

Oligodendrogliomas develop from special glial cells called oligodendrocyte and occur mostly in the frontal or temporal lobes of the cerebrum. These type of tumors account for 4% of all primary brain tumors and 12 to 20% of gliomas. They tend to diffuse into the surrounding tissue, which makes them difficult to completely remove.

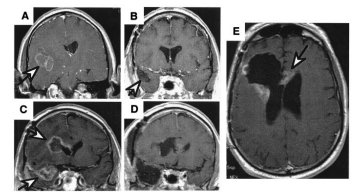

Figure 2.3. *MR image of GBM Illustrates the spread of disease. (A) Arrow points to the GBM before surgery. (B) Scan after gross total resection with surgery following radiation therapy. (C) Recurrence of disease 6 months after surgery and not only in the resection margin also in frontal lobe. (D) Scan after resection of both recurrent tumors. (E) 3 months later,illustrating the tumor recurring at the resection margin. Image is adapted from [13].*

2.2.1 Glioblastoma

Glioblastoma multiform (GBM) is a grade IV astrocytoma, and the most aggressive primary brain tumor in adults [9]. GBM can be classified as primary and secondary. Primary GBM covers 60% of the cases in adults over 50 years of age, while the secondary accounts for the rest, has a slower growth pattern and occurs more in younger patients. GBM is mostly found in the supratentorial white matter of the cerebral hemispheres, and can invade into the gray matter. It can, however, occur in any lobe of the brain. GBM, as is understood from the name, has a variable histopathology. It is composed of many heterogenous mixtures of cells and tends to spread aggressively. The prognosis for patients with GBM is not good, as it is associated with fast growth. Without therapy, patients die within three months and with optimal therapy, have a mean survival of approximately 12 months [1].

2.3 Present alternatives to the surgical diagnosis and resection of brain tumors

Imaging studies are essential in order to locate and diagnose GBM. A computed tomography (CT) scan is an efficient way to determine the location and size of a tumor. This technique may, however, fail in depicting all multifocal lesions. Magnetic resonance imaging (MRI) has a higher confidence in revealing detailed information of the brain and diagnoses 92% of all malignant gliomas [12]. Positron emission tomography (PET) and magnetic resonance spectroscopy (MRS) are also useful to detect recurring brain tumors. The complex characteristics of brain tumors and their infiltrative growth into the surrounding tissue make it difficult to locate all tumors, and this is one of the reasons the tumors are resistant to conventional therapies, see Fig.2.3.

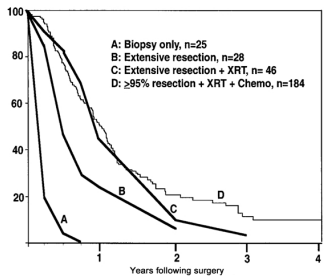

Figure 2.4. *Kaplan-Meier overal survival curves for GBM diagnosed patient. (Image is adapted from [13]).*

The first treatment step is, in most cases, surgical resection of as much of the tumor as possible. This initial treatment is almost always followed by radiation therapy and chemotherapy. In general, even after a successful tumor removal and with respect to all treatment modalities, the median survival of this disease ranges from 2-3 months to 1 year, see Fig. 2.4 [13]. Stummer *et al.* reported a correlation between extent of resection and survival with a survival advantage of 5 months [14]. This poor outcome has drawn significant attention to using intraoperative modalities to enable improved resection during surgery. The spatial shift in the position of the brain due to change in intracranial pressure when opening the skull during surgery decreases the usefulness of preoperative imaging. Several techniques, including CT, MRI, neuronavigation, ultrasound, and fluorescence guided resection (FGR) are the intraoperative modalities used today.

Intraoperative MRI and CT: CT provides a direct image of the clinical situation of the patients. A CT navigation procedure takes place on a CT table in real time to assist the neurosurgeon reach the deep lesion [15]. Intraoperative MRI (iMRI) presents a better surgical outcome as a result of better soft tissue contrast and higher resolution using high-field iMRI. The high cost of this technology can, however, be an obstacle.

Intraoperative ultrasound: This modality has an advantage over MRI in being inexpensive and portable. Like MRI it does not need to use ionizing radiation and can be used by neurosurgeon without assistance. Intraoperative ultrasound can have rather poor tissue contrast and is difficult to use for deep lesions [16].

Fluorescence guided resection (FGR): This new technique has recently been introduced to provide a direct optical identification of glioblastoma tissue. The technique usually employs a fluorescent contrast agent to label the malignant tissue. This contrast agent is administered systemically prior to the surgery. Usually δ-aminolevulinic acid (ALA)-induced protoporphyrin IX (PpIX) is employed as a contrast agent. Its selectivity is based on the fact that the blood-brain barrier (BBB) is broken in tumor tissue and ALA is not able to cross intact BBB [17]. Altered pattern of enzyme activity [18, 19] and limited availability of iron level in tumor cells [20] are also parameters contribute in ALA uptake in brain tumors. Further reasons for selective accumulation of PpIX within tumor cells is still subject to investigate. Thus far, results indicate that FGR is feasible, promising, and it has proven to be significant in delineating tumor margins. The technique is partly limited insofar as that only superficial

tissue can be visualized, and only when the ambient surgical light is switched to violet light excitation.

Neuronavigation: Intraoperative neuronavigation is usually used in combination with high-resolution pre-operative imaging modalities. This combination of information provides the surgeon with the ability to see the target point accurately in the brain in three dimensions.

Chapter 3

Biomedical Optics

When light interacts with matter in a sample, different processes or phenomena can occur. They all lead to an alteration in the light field and can transfer energy between the light to field and the matter. This chapter outlines the different light tissue interaction mechanisms, either as surface properties, such as reflection, or volume effects such as scattering and absorption. Thereafter, fluorescence and its capability in biomedical diagnostics are presented.

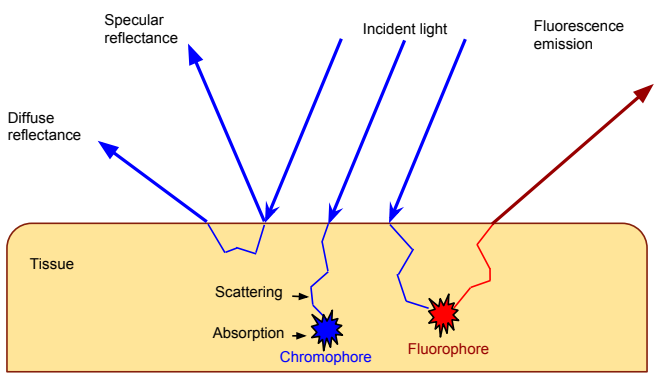

Figure 3.1. *Schematic presentation of the interaction between light and tissue.*

3.1 Reflection

When light impinges on a surface of a medium, it will partly be reflected in and partly transmitted through the surface. This inter-

actions is due to a difference in refractive index of the two media, and is governed by the Fresnel reflection laws. The reflected light has a mirrored propagation direction. This light is called specular reflected light. The light transmitted through the surface will be refracted according to the Snell's law and the light direction is thus slightly altered. Most of the light transmitted through the surface of a biological sample into the medium will be scattered one or multiple times in the medium (see Fig.3.1). Some of that scattered light will escape the medium. This light is called diffusely reflected light.

3.2 Absorption

When light is incident on tissue composed of different molecules, it can be absorbed by various chromophores. Chromophores are defined as molecules that can absorb visible light. Here we extend the definition to include also molecules that can absorb near-infrared light. The property of these molecules to absorb light is given by the energy level structure of that molecule, having an excited energy level at a position matching the energy of the photon that can be absorbed. This absorption phenomenon results in transferring the energy of a photon to the absorbing molecule, while the molecule makes a transition from the ground energy state to an excited energy state. This thus leads to a reduction in the intensity of the light within the tissue. The intensity of a light beam in an absorbing medium can be expressed by the Beer-Lambert law:

$$I_T = I_0 * exp(-\mu_a d).$$

When μ_a is the probability of light absorption by tissue molecules per unit path length, while d is the path length of the light within the medium. The absorption of light is strongly dependant to the wavelength, see Fig. 3.2. As can bee seen in the figure, in the approximate wavelength region between 600-1300 nm, the total absorption is relatively low. This wavelength region is called the tissue optical window, and is used for many diagnostic and therapeutic purposes, since the tissue is more transparent and this will provide possibility to reach deep targets in tissue due to good light penetration. The most important absorbers in biological tissues will be discussed in the following .

Water is the most abundant chemical compound of our body, accounting for approximately 2/3 of total body mass. As such, it can be considered a strong absorber in the tissue, especially outside the visible region of the light spectrum. The absorption coefficient of water is low within the tissue optical window and has a first distinct absorption peak at 980 nm. Above this wavelength, the absorption starts to increase

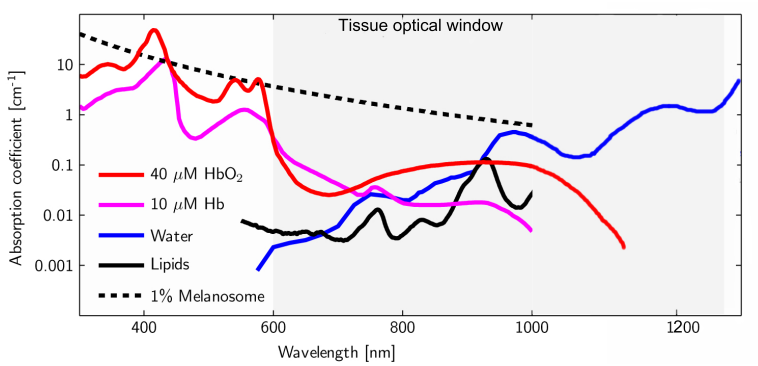

Figure 3.2. *Absorption spectra of the main tissue chromophores. Image is adapted from [21].*

fairly rapidly in the infrared (IR) region and continues to increase at longer wavelength into the mid-infrared.

Haemoglobin is an iron-containing protein in the blood with the function to carry oxygen from the lungs to the tissue. Both oxyhemoglobin and deoxyhemoglobin are dominant absorbers of light in the visible wavelength region. Differences in spectral in absorption features of these two forms can be utilized to measure changes in hemoglobin saturation and tissue oxygenation.

Melanin is a dark pigment, giving the hair, skin, and the iris its natural colors, and has an absorption peak around 335 nm. The absorption then decreases slowly with wavelength throughout the entire visible spectral region. Melanin can also be found in other organs, e.g. inside of eye [22] and in brain [23].

Lipids have less significant contribution in the visible wavelength spectrum. Similar to the water, in the Near-infrared (NIR) region the absorption cannot be neglected.

3.3 Scattering

Scattering of light in turbid media occurs due to mismatches between refractive indices of different small structures in the medium. In tissue different cellular structures, mainly mitochondria and nuclei [24] exhibit different refractive indices and give rise to light scattering, changing its direction. The interested reader is referred to Popp *et al.* [25] for detailed information about the microscopic origin of light scattering in tissue. Two tissue parameters can

be used to describe this phenomena, the scattering coefficient μ_s and the anisotropy factor g. The scattering coefficient defines the fraction of light scattered per unit of length, while the anisotropy factor $g =< cos\theta >$, where θ is the scattering angle, determines the degree of forward scattering in each individual scattering event. If the scattering is isotropic, g is equal to zero. The g-value depends on the size and refractive index of the scattering structures, and it tends to become close to unity when the size of the scattering structures becomes large in comparison to the wavelength of the light. The case of highly scattering tissue, when light becomes diffuse from multiple scattering events, a reduced scattering coefficient μ_s can be derived by combing this two quantities.

$$\mu_s' = (1 - g)\mu_s$$

The scattering in tissue is typically dominated by Mie scattering, since the size of the particles is larger than the light wavelength. The wavelength dependance for Mie scattering can be expressed by the following expression:

$$\mu_s' = a_M.\lambda^{-b},$$

where the coefficient $b > 0$ is related to the particle size and a_M is scattering amplitude linked to the density of scatterer particles in the tissue. As the particle size decreases to become smaller than the light wavelength, Rayleigh scattering dominates. For this the wavelength dependence is:

$$\mu_s' \propto \lambda^{-4}.$$

Based on these two scattering effects, there is a more general expression for tissue scattering,

$$\mu_s' = a\lambda^{-b}.$$

3.4 Fluorescence

Transitions between energy states of atoms and molecules frequently occur by photon processes such as absorption and emission. Once a fluorescent molecule is excited due to the absorption of light, a number of things can occur. One possibility is that the molecule returns to the ground state from the lowest vibrational level of an excited singlet state and emits light with longer wavelength, lower photon energy as compared to the excitation light that is, fluorescence, see Fig. 3.3. Fluorescent molecules are called fluorophores or fluorochromes. The spectral difference between the excitation and emission wavelength is called the Stokes shift. The molecule-specific Stokes shift is a key property that allows fluorescent molecules to be identified and utilized for tissue diagnostics.

This is particularly important in multiplex fluorescence application, because the emitted light from one fluorophore may excite another one within the sample.

Fluorescence is a short-lived luminescence event, with a fluorescence lifetime in the order of ns. Each fluorophore has a characteristic absorption and emission spectrum. The excitation can occur at several wavelengths, with one wavelength yielding the highest fluorescence emission. This is, not surprisingly, called the excitation peak. Similarly, the wavelength of the strongest emission is called emission peak. An intrinsic property of fluorophore is the fluorescence quantum yield (Φ). It is a probability type of function defined as the ratio of the number of fluorescence photons emitted to the number of excitation photons absorbed. Another important property of the fluorophore is whether it is prone to photobleaching. During a prolonged exposure or a high intensity excitation light, the fluorescence quantum yield may decrease - photobleaching. Photobleaching is an irreversible photochemical destruction of the fluorophore. The molar extinction coefficient (ϵ) is yet another intrinsic property of a fluorophore, defined as the probability for light absorption per unit path-length of light at a given wavelength for one molar concentration of the fluorophore. The product of the two quantities, fluorescence quantum yield (Φ) and extinction coefficient (ϵ), represents the brightness of a fluorophore.

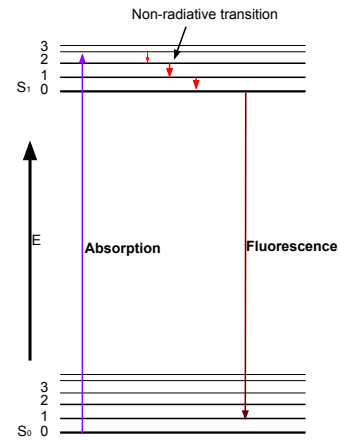

Figure 3.3. *Jablonski diagram of fluorescence event.*

3.4.1 Autofluorescence

The autofluorescence, or endogenous tissue fluorescence, is defined as fluorescence emission of unstained biological structure under UV or visible light irradiation. The emission spectra of this endogenous fluorescence is broad with overlapping contributions from several fluorophores, making it difficult to separate contribution of different fluorophore. The fluorescence emission spectra of most abundant natural fluorophores can bee seen in Fig. 3.4.

NADH (nicotinamide adenine dinucleotide) and FAD (flavin adenine dinucleotide) are two coenzymes involved in several important reactions in the cell metabolism. The fluorescence properties of the reduced form of NADH differ from that of the non-reduced form NAD+, and is thus an indicator of the metabolic state of the tissue. By detecting the level of NADH by means of its fluorescence emission, one can get information valuable in the diagnostics of malignant disease. Similar information can be obtained from the fluorescence of the flavin.

Collagen and elastin are the most important structural protein maintaining the firmness and elasticity of tissue, respectively.

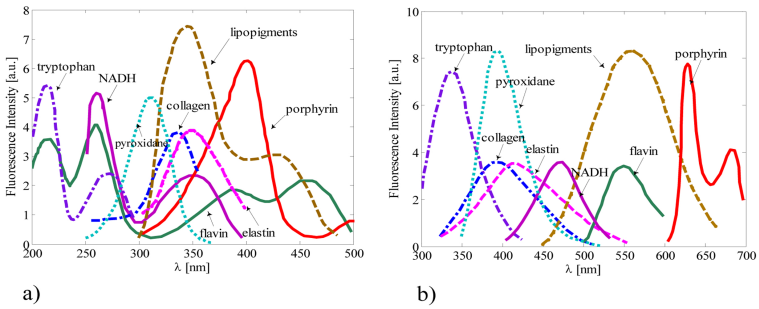

Figure 3.4. *a) Absorption and b) emission spectra of some tissue fluorophores. The graph is adapted from [26].*

The fluorescence emission of collagen and elastin is associated with connective tissue and can be used to differentiate between various tissue types and to characterize tissue pathologies [27].

Tryptophan is an amino acid present in all cells and the most common tissue fluorophore in tissue.

Porphyrin are molecules in the body that combine iron to produce heme. The porphyrin fluorescence emission is in the red spectral range.

Table 3.1: Main endogenous fluorophores in tissue [28]

Fluorophore	Excitation maxima (nm)	Emission maxima (nm)
NADH [29]	290, 320-360	440-460
Collagen	325, 360	395-405
Elastin	290, 325	340-400
FAD [30]	365, 450	535
tryptophan	280	350
Porphyrin	400-450	630-690

Tissue autofluorescence can be used to distinguish different types and states of tissue and as a criterion for tissue diagnostics.

Table 3.1 gives the excitation and emission wavelength for the most important tissue fluorophores.

3.4.2 Fluorescent tumor markers

In order to enhance the sensitivity and specificity of fluorescence tumor diagnostics, fluorescent tumor markers are frequently employed as exogenous fluorophores. An important characteristic of these tumor-seeking markers are their selective accumulation in the malignant or pre-malignant tissue following drug administration - topically or systemically (the latter through injection or orally). A suitable tumor marker needs to have a higher selectivity for malignant tissue and a rapid accumulation after administration. Another property of a fluorescent tumor marker is an intense and specific fluorescence emission following light excitation. A high fluorescence yield with narrow emission spectrum, preferably in the red region, makes it possible to easily be distinguished from the tissue autofluorescence, and also helps to improve diagnostics of a malignancy. In some cases the same substance can also be used as a photosensitizer for treatment of the malignant tumor utilizing photodynamic therapy (PDT). In PDT, the photosensitizer molecules absorb the specific treatment light, whereupon reactive oxygen species are produced, killing nearby cells.

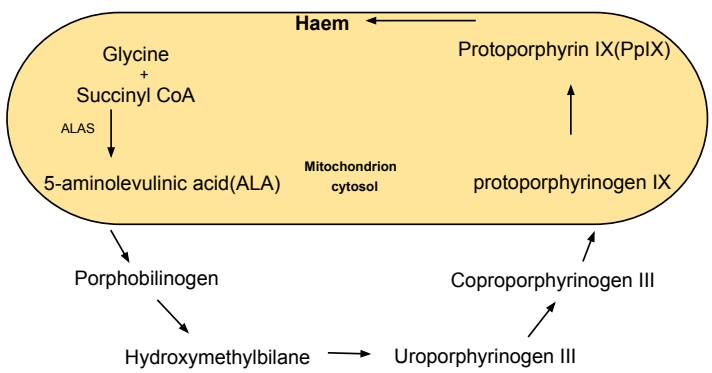

Figure 3.5. *Eight steps in the heme biosynthesis pathway.*

Among all fluorescent tumor markers, 5-aminoleuvulinic acid (ALA) induced-protoporphyrin IX (PpIX) is most widely used. ALA is an endogenous amino acid essential for the heme biosynthesis pathway, see Fig. 3.5. Heme biosynthesis begins by producing ALA in the mitochondrion, while the final product is formed by insertion of a ferrous ion in PpIX by the help of the ferrochetalase (FC) enzyme. When an excessive amount of ALA is administered to the system, FC isn't able to directly convert all produced PpIX to heme, which results in a temporary accumulation of PpIX in

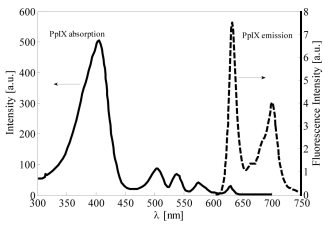

Figure 3.6. *Absorption and emission spectra of PpIX.*

the cells [31]. The selectively higher accumulation of PpIX in malignant cells can be explained by the disrupted BBB, differences in activity of enzymes contributed in heme biosynthesis and lower availability of iron in tumor cells. Many studies are performed in order better to understand this process [17–20].

The tumor concentration of PpIX reaches its maximum within 1-6 hours, depending on tumor type, after oral intake or intravenous injection of ALA. Fig. 3.6 shows the absorption and emission spectra of PpIX.

An important clinical study using ALA for guiding brain tumor resection was presented by Stummer *et al.* [32–34]. Protoporphyrin IX was induced by administering a dose of 20 mg/kg body weight ALA prior to intraoperative fluorescence microscopy guidance during surgery. The outcome of this work was a specific improvement of gross total resection in high grade glioma surgery.

3.4.3 Multivariate analysis of fluorescence data

Multivariate analysis are widely used to evaluate data sets with large and complex amount of information with more than one variables. Depending on the data set and the information requested, different multivariate analysis methods can be employed. If the collected data set comprises several measurements, principal components analysis (PCA), correspondence analysis (CA), and multidimensional scaling (MDS) can be used. Among these techniques, PCA is the oldest and most popular method. The goal of PCA is to decompose the data set by reducing the number of dimension, while minimizing any loss of information.

In the case of more than one data set, when one set contains independent variables (or predictors) and the second data set corresponds to dependent variables (or responses), partial least square (PLS), principal component regression (PCR), and multiple linear regression analysis (MLVR) are the most frequently used methods for tissue fluorescence spectroscopy. PLS is useful when a set of dependent variables needs to be predicted from a large set of independent variables. In fact, PLS extract a linear combination of the predictors with the best correlation with responses but doesn't provide any information about underlying relationship between variables. PLS is believed to be the more optimal method for concentration prediction [35]. When the number of predictor variables are more than responses, the data will be over-fitted which leads to a poor prediction of the property of interest (*e.g.* concentration in this thesis work). Validation methods enables to avoid over-fitting by dividing the data set into two parts, training set used to create a fitting model and validating set used to evaluate the prediction test response. One of the most common forms of cross validation is Leave-one-out cross-validation (LOOCV), where only one single observation is used as the validation set and the

remaining are used as the training set. An average square error is computed to evaluate the model.

Chapter 4

Experimental setup

This work implements a novel approach to fluorescence guided resection of the most malignant brain tumor, GBM. This chapter reports on development of system design, its technical specification, the light modulation and methods for processing signals, and samples description used in this study.

4.1 System specifications

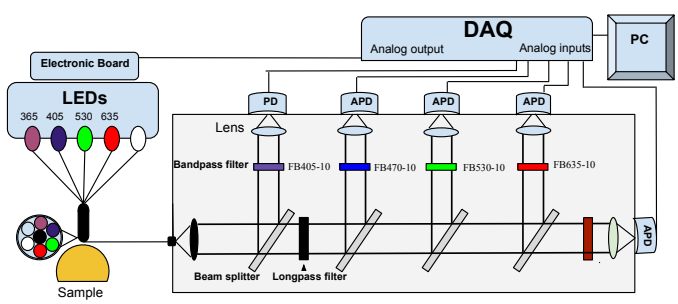

Figure 4.1. *Schematic representation of the system.*

The system developed with the purpose to be useful for guiding brain tumor resections is outlined in Fig 4.1, including a schematic illustration of the distal end of the fiber-optic probe. It has three main parts: A light source, a fiber optical probe and a detector unit. The light source (Prizmatix Ltd.) consists of five

light-emitting diodes (LED) at four different wavelengths: 365nm, 405nm, 530nm, 635nm as well as a white light LED. The UV light (365 nm) is used to excite endogenous fluorophores in tissue, while the violet light (405 nm) serves as an excitation source for PpIX. The other wavelengths and the white light are used to provide reflection data and thus signals correlating with optical properties from the tissue at these wavelengths. The maximal output power of each LED is approximately 10 mW. The intensity of the light is adjustable to avoid saturation on the photo detectors (and also minimize photobleaching).

The light source is controlled by the output ports of a 16-bit data acquisition (DAQ) board (Supplier, Type No. USB6351). A labview program controls the light generation sequences and time intervals between the on (high voltage) and off (low voltage) mode of the LEDs. For this purpose, a custom made electrical board was designed and connected to the Digital Clock (CTR) output channel of the DAQ board.

The hand-held fiber-optical probe delivers light to the sample by five optical fibers each with a core diameter of 750 μm, a numerical aperture of 0.5 and a length of 4 meters suitable for the operating room. The optical fiber located in the center of probe is used to collect fluorescence and diffusely reflected light from the sample and guides the collected light to the detection unit. There is a fiber collimator (Edmund Optics; 64770) in front of the detection unit. The collimated light is split into five different light paths by means of four dichroic beam splitters (BS) (Thorlabs; DMPL425, 505, 567, and 638, respectively). The detector after the first beam splitter is a silicon photodiode (PD) (Edmund Optics; 53378). This is employed to detect diffusely reflected UV and violet light from the probed tissue. Four avalanche photodiodes (APD) (Hamamatsu; S9075), are used to detect the collected endogenous fluorescence light, exogenous PpIX-fluorescence and its photobleaching products, and also reflectance from the red, green and white LED. To suppress the strong diffusely reflected UV and violet light from reaching the APDs, a long pass cutoff filter (3 mm Schott GG-435) is mounted after the first elastic channel. Bandpass filters (Edmund Optics; FB405-10, FB470-10, FB530-10, FB-635-10, and FB-660-10, respectively) are mounted in front of each detector to transmit only the desired spectral band of light to each detector. The bandpass filters are followed by a lens to focus the light onto the center of the active area of the detectors. The photocurrents from the photodetectors are first converted to voltages by five trans impedance amplifiers, one for each detector, transmitted to five analogue inputs of the DAQ board and then sent to the computer. Real-time control and initial data analysis is performed in LabView (Version 2012, National Instruments).

4.2 Signal processing

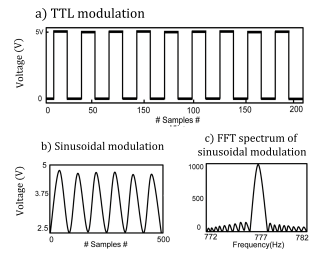

Figure 4.2. *a) TTL Pulse applied on one LED. b) The sinusoidal wave applied on one LED. c) FFT spectrum from the detected fluorescence and reflectance light.*

Light intensity modulation has been employed in the data acquisition for two reasons. Firstly, it was important to measure the signals generated for the five LEDs independently. Secondly it was essential to enable measurements in strong ambient light conditions. Two different periodic waveforms: square-wave modulation and sinusoidal-wave modulation, have been evaluated to modulate the light from the source in this system. The square wave modulation is based on a TTL signal generated from the CTR port of the DAQ board, (see Fig. 4.2.a). A series of square wave pulses is created with a varied voltage sequence with square wave voltage pulses between 0 (low) and 5V (high) at a frequency of 777 Hz. The resulting waveform from the square wave modulation consists of a 777 Hz repeated time sequence of 11 time slots. This sequence includes one time slot where each of the LEDs is on at maximum and reduced power, respectively, and one where they are all switched off. The main reason to apply voltage in high and low power is to monitoring the power fluctuation resulted from temperature variation of LEDs. For each detection channel, the average signal value within each of these time slots is calculated and then subtracted from the average value when all LEDs are switched off. In order to increase the signal-to-noise ratio, this sequence is repeated over 70 cycles and an average value was calculated, corresponding to a 90 ms integration time.

In sinus modulation, only the bue LED was used. The light was driven by a sinusoidal wave at 777 Hz with a modulation amplitude of 2.5V. Such a modulation wave is illustrated in Fig. 4.2.b). The fast fourier transfer (FFT) of the recorded signal is used to distinguish the frequency components of the detected signal. The FFT spectrum is integrated over a frequency interval covering the peak at 777Hz and also any signal contribution from the ambient light is measured as a sum of all signals in the frequency interval 0-110 Hz, again averaged over 90 ms integration time. A typical example of the FTT spectrum of a sinus wave is illustrated in Fig. 4.2.c).

4.3 Samples

In order to validate and test the system performance, water-based tissue phantoms were prepared. The tissue phantom employed in this study was based on three major ingredients, an absorber, a scatterer and a fluorophore. Diluted Intralipid (Fresenius Kabi, Sweden; 200 mg/ml), which is a fat emulsion, was added to provide the required scattering properties, while diluted India ink (Pelican Fount, Germany; 1:100 stock solution prepared in our lab) with a minimal influence on phantom scattering and high contribution

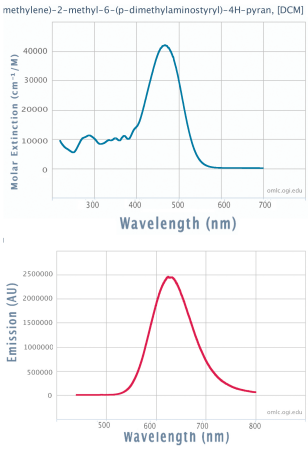

Figure 4.3. . *Absorption and emission spectra of DCM. Image adapted from [36].*

to the absorbtion, or bovine blood (purchased from a local supermarket), was used as absorbers. The DCM or PpIX (Fisher Scientific) with similar fluorophore brightness and fluorescence emission spectra properties was served as a fluorophore. DCM, which is a strongly fluorescence dye with a very broad absorption spectrum, can be excited using light at 470 nm. The excitation and emission spectra of DCM are presented in Fig. 4.3. In order better to control and suppress any aggregation of PpIX in the phantom, the surfactant tween (Scharlau Chemie) was mixed into the phantom. The phantoms were designed to mimic the optical properties of gray matter of brain tissue (See table 4.1).

Table 4.1: Tissue phantom substances composition by volume percentage

Substance	Water (%)	Intralipid (%)	Ink (1:100 stock solution) or Blood (%)
Volume	96	3.5	0.5

Chapter 5

Experimental system validation

The developed system was designed to quantify the fluorescence signals during glioblastoma resection surgery using ALA-induced PpIX as the tumor marker. A set of tissue phantoms were prepared to study the sensitivity and linearity of the system as well as the ability to suppress ambient room light in the detection. The tissue phantoms used in this study are described in chapter 4.

5.1 System linearity assessment

Several sets of experiments were carried out to validate our setup. First only 405nm excitation light was used for studies on system validation of linearity response in a dark room as well as under well controlled ambient light conditions. This wavelength matches the absorption thus is able to excite PpIX. The 405nm excitation light also overlaps with the absorption of DCM, enabling this light source to induce DCM fluorescence. Two amplitude methods, sinusoidal and square wave modulation, were employed for their ability to suppress any ambient light in the laboratory room. In the first series of experiments liquid phantoms were prepared by mixing 3.5% volume of Intralipid, 0.5% of Ink (1:100 stock solution) and 96% water. The fluorescence features of the phantoms were manipulated using DCM as a fluorophore. In order to obtain a 100 μM DCM solution, 0.015 g DCM (the molar weight is 303.37 g/mol) was dissolved in 0.5 L water and solubilized in ultrasonic bath. The phantom with the highest fluorophore concentration was prepared in a glass cylinder container. The lower concentrations have subsequently been prepared by diluting with the initial tissue phantom, without any fluorophore. Similarly, fluorophore concentrations ranging between 25 and 1000 nM were prepared. A gentle stirring of the sample during measurement was employed to prevent the fluorophores from aggregation and to minimize the

photobleaching so that the bleached dye molecules directly under the tip of the delivering fiber were continuously replaced by fresh fluorophores. Whereas these initial results were promising, new samples containing PpIX instead of DCM as a fluorophore were prepared to investigate the lower detection limit of PpIX florescence. PpIX powder (0.056 g) was dissolved in 20 mL of DMSO and 80 mL of distilled water was added to obtain a 1 mM PpIX stock solution. The fluorophore concentration in the tissue phantom was, in this series of measurements, varied in the same way as before between 10 to 100 nM. Bovine blood (3% in volume) instead of ink was used as absorbers to have a realistic wavelength dependence in comparison to human tissue.

5.1.1 Result of linearity tests

The measured data need to be corrected to account for any small variation in source power. For this purpose, the ratio between fluorescence and reflection signals was formed. Figure 5.1 shows the results from the first set of measurements. The ratio has a very linear dependence on the fluorophore concentration for both the square and sine wave modulations using 405 nm LED as an excitation source.

There was a negligible difference in sinusoidal and square wave modulation in this course of the experiment. The work has shown that very low fluorescence concentration is detectable by this system, much lower concentrations than is expected in brain tissue during clinical use [37].

5.2 Ambient light suppression

As mentioned in the Introduction, the previous generation of this setup (OTP) [3] was sensitive to the ambient light during the measurements, such as fluorescence microscope lamp and room light in the operating room. In order to evaluate the capability of suppressing ambient light with the present system, measurements were conducted with tissue phantoms under well controlled ambient light conditions. In this study we used a white light ring-lamp from a microscope with similar emission spectrum to the surgical operating microscope, to examine the influence of different light conditions on the recorded signals. A tissue phantom (Similar composition to 4.1) with 100 nM PpIX concentration was prepared and the ring light was located at varying distances vertically above the sample to provide an even illumination of different intensities. A lightmeter was used to quantitatively determine the ring light intensity at the surface of the tissue phantom. The experiment started with a 60 centimeter distance from the sample. The distance was then decreased to obtain a stronger ambient light condition. Both types

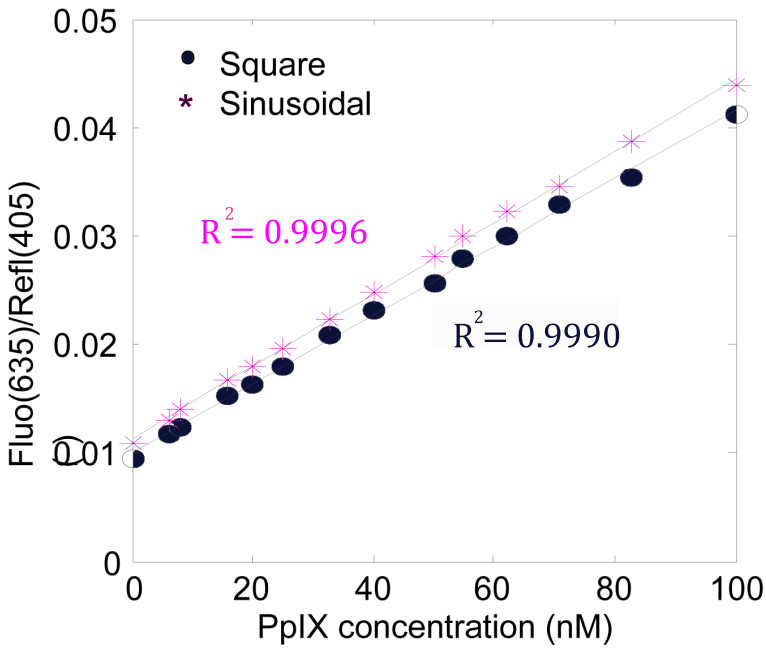

Figure 5.1. *PpIX quantification using violet light from two modulation techniques. The solid line indicates a linear fit to the data.*

of modulations were applied to investigate the capability of ambient light suppression.

5.2.1 Result

Figure 5.2 illustrates the results, including raw data, for different ambient light conditions. Since the ambient light has the modulations in the low frequency range (0-100 Hz), the detected signal with a modulation at 777 Hz is totally related to the light from the LED source. In square modulation the low frequency wavy shape of the raw data curves is related to the ring light while the relatively small pulses were produced from the 777 Hz frequency-modulated LED. Figure 5.2.b) illustrates the evaluated signal level as a function of the ambient light intensity. In figure 5.2.c), the on-off lock-in type of subtraction was performed for the 777 Hz modulation to remove the influence of the ambient light. As mentioned in the experimental setup chapter, the average signal value was for these plots calculated over 70 cycles to increase the signal-to-noise ratio. The results clearly indicate that the measured signal is almost completely dominated by the ambient light,

while the fluorescence signal could be recovered almost uninfluenced by the ambient light when the lock-in type of subtraction was performed. Comparing the results of this experiment and previous experiment, no remarkable difference was observed between two modulation schemes so that the square modulation has been picked to process signals afterwards.

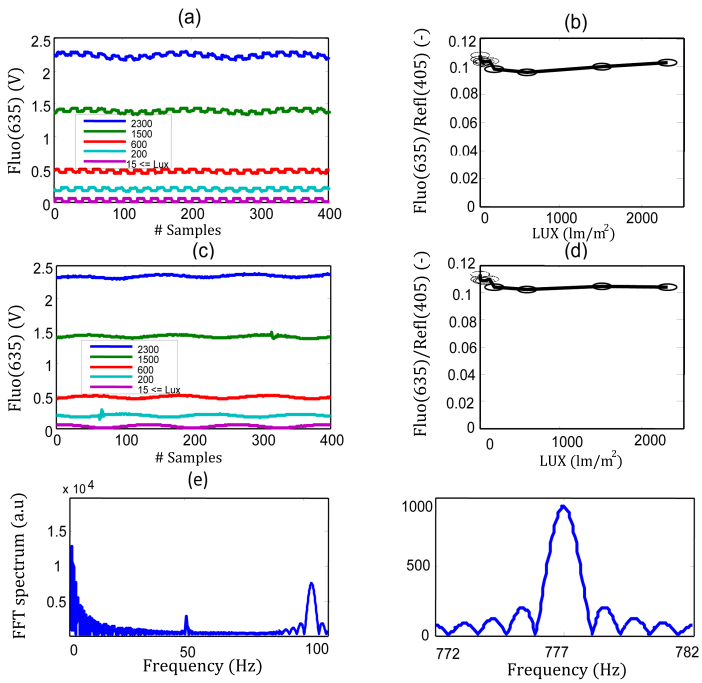

Figure 5.2. *Sensitivity of the system to the ambient light level for a fixed PpIX concentration of 100 nM. Figures (a) and (c) show the raw data when the violet light was modulated by a square and sinusoidal waves, respectively. (b) and (d) demonstrate the fluorescence vs reflection ratio (i.e. the evaluated signal corresponding to the PpIX concentration) in different ambient light conditions for the two modulation schemes. (e) presents the FFT spectrum of sinusoidal modulation with peaks related to ambient light (below 100 Hz) and light from the excitation source (777 Hz).*

5.3 Evaluation protocol

Now, after having been able to successfully demonstrate the capability of suppressing any influence of ambient light on the detected

signal using one 405 nm excitation source, all channels were connected. The multiple LEDs were run sequentially using an electrical board (multiplexer) connected to the DAQ board. In order to evaluate the experimental data, multivariate analysis is used in the data processing. The partial least squares (PLS) method was employed to develop a linear model of sample fluorescence and optical properties from 269 different samples varied in known dependent variables such as absorption, scattering and fluorescence. Intralipid concentration varies between 3% -8% of the whole phantom volume, while 0%-4% of the blood concentration was considered as an absorption variation. Protoporphyrin concentration was varied between 0 to 1000 nM. The samples were prepared through several dilution steps starting from the highest concentration. It was diluted into the lowest concentration and the last sample was measured in a separate container without any fluorophore. The measurement process occurs similarly to the previous experiment. For the PLS model regression, data normalization was done and a data matrix was created. This model can be used to predict the fluorescence concentration in unknown samples in the future, as long as the absorption, scattering and fluorescence properties fall into the interval of this set of samples. Leave-one-out methodology was used to evaluate the accuracy of predicting the fluorophore concentrations. LOO-CV split the dataset into two groups, it left one observation as the validation data, and the remaining observations were used to build the PLS regression model and this was repeated so that each variable was used as validation data.

5.3.1 Result

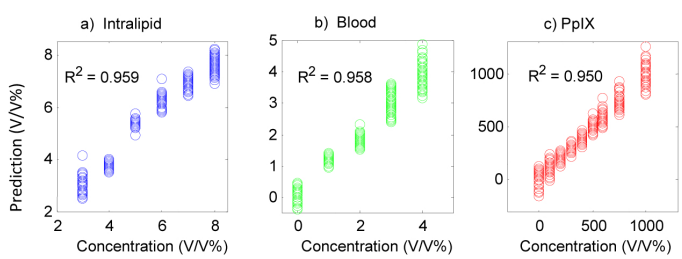

Figure 5.3. *PpIX quantification in liquid phantom with various optical properties. a) Predicted Intralipid concentration b) Predicted blood concentration and c) Predicted PpIX concentration.*

Linear regression analysis was performed using the data from all sample measures to correlate between predicted and true prop-

erties for different variables. Figure 5.3 illustrates the relation between these values and also indicates their coefficient of determination (R^2). This coefficient denotes the goodness of linear relation between responds and predicted values. As can be seen, the estimated blood and intralipid concentration are highly correlated with correlation coefficient of 0.96 and 0.96, respectively. For fluorescence concentration, the correlation coefficient is 0.95. The result shows the viability of PLS regression for intralipid/scattering, blood/absorption, and PpIX fluorescence concentration estimation using the multi-LEDs arrangement. It was recognized that there was an instability in the APDs temperature since it is well known that APD gain is very sensitive to ambient temperature.

5.3.2 Temperature compensation

The APD's high sensitivity and wide bandwidth makes it widely used as a detector for optical measurements. The temperature dependence of APD is a disadvantage and needs to be compensated to achieve a stable output. The first attempt to overcome this issue was to prepare a solid phantom as a reference. This reference was measured before and after each experiment. The obtained data can be normalized through dividing by this value. A temperature calibration was also performed to get improved outcome by monitoring the temperature variation and deriving the temperature coefficient. In this study, thermistor coupled to each APD allowed accurate monitoring of temperature during the measurement. The temperature coefficient can be found and applied to output voltages to correct the temperature dependence.

Chapter 6

In vivo experiments

In order to ensure that the system will work in complex living systems, an in vivo clinical human trial was performed. Skin tumors are easily accessible and such tumors were used in this first clinical trial. The whole setup was packed on to a portable case for outpatient clinical data acquisition and carried to the clinic of Dermatology at Skåne University Hospital in Lund.

6.1 Materials and Methods

The fluorescence and reflectance spectroscopy system has previously been described in chapter 4 and 5. The measurement was carried out on 22 patients with skin tumors. Among patients with different types of skin tumors, eight were treated by photodynamic therapy (PDT). These patients received a topical dose of ALA (Amelux 78 mg/g and Metvix 160mg/g) in the cream 3 hours before PDT. To investigate the effect of ALA on tumors, three different cases were considered. In the first case the measurement was performed prior ALA administration. In the second case the data was captured before the treatment and in the last case it occurred after PDT. To allow intersubject data analysis, optical fiber was placed at four points outside of the lesion, two on the border and rest inside of the lesion. This protocol could, however, not be fully followed for all patients due to the limited size of the tumor. For patients without PDT, the measurements were carried out in order to investigate the tissue autofluorescence and diffuse reflectance variation within the tumor and healthy tissue. The excitation light used for autofluorescence is UV light and the data is normalized to the reflection (405 nm detection channel) so as to compensate the variation of light source intensity. At the 365 nm excitation wavelength, most of autofluorescence arises from NADH and flavin coenzymes which have emission at 420-470 nm [30]. Be-

a)

b)

Figure 6.1. *A typical skin tumor*

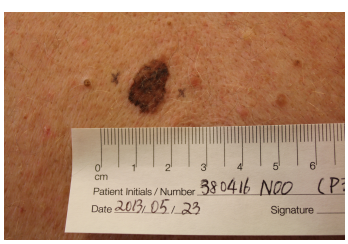

Figure 6.4. *A malignant melanoma on the upper back.*

fore and after each measurement, the signal from a stable reference was also acquired, to allow a compensation for any temperature or other drifts in the system.

6.2 Result

Figure 6.2 presents one of the eight measurements (see Fig. 6.4) of the different experiments conducted on patients with skin tumor undergoing PDT. The PpIX accumulation at the site of application in the skin tumor is obvious from the results presented in the figure 6.2. In this case it was straight forward to detect the lesion in the turbid tissue with a robust distinction. The curve after PDT evidences PpIX existence after treatment which indicates a somewhat prolonged photosensitivity of this drug in the lesion.

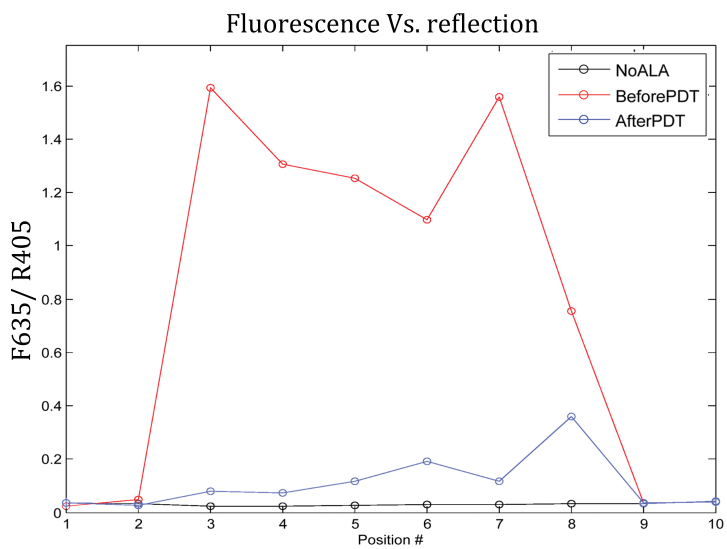

Figure 6.2. *In vivo fluorescence reflectance spectroscopy of a patient with a skin tumor before ALA administration, before PDT and after PDT.*

The result of autofluorescence emission from endogenous fluorophore of one patient, among 14 patients were not treated with the PDT, is demonstrated in FIG 6.3. This tumor is diagnosed as a malignant melanoma (See in Fig. 6.4). It shows the system ability to distinguish between normal and tumors tissue by only using the tissue autofluorescence.

In summary, significant differences have been noted between optical properties of different types of tissue. This is the wealth of

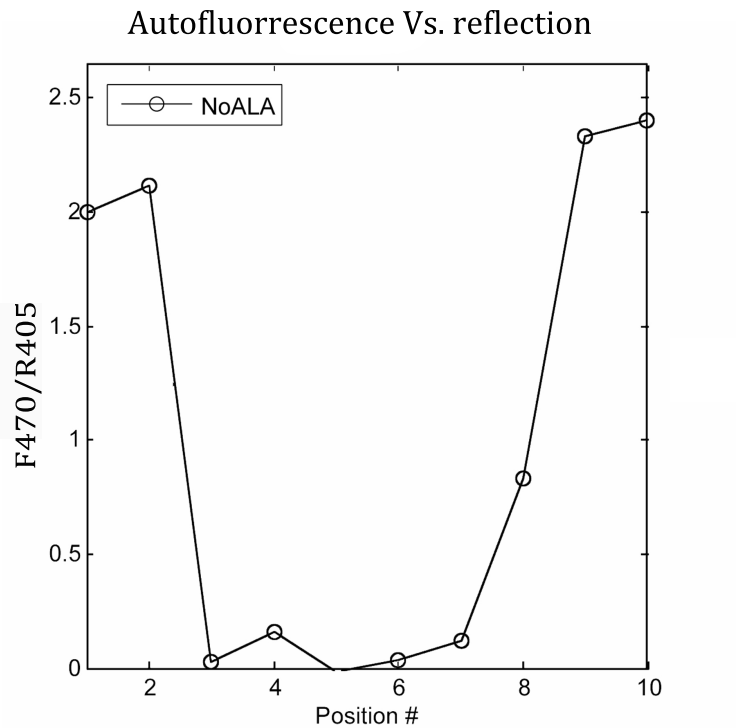

Figure 6.3. *In vivo autofluorescence reflectance spectroscopy of patient with malignant melanoma skin tumor.*

this study that supports the use of both endogenous and exogenous fluorescence in the biomedical optical applications. A further evaluation on complete data is proceeding to evaluate the diagnostic potential of this spectroscopic system in classifying different skin lesions.

Chapter 7

Discussion and outlook

A novel combined fluorescence reflectance spectroscopy system based on LED-excitation and APD-detection has been developed and evaluated. The system is built as an intraoperative guiding tool for resection of glioblastoma, the most frequent and complex to treat the malignant brain tumor. The LEDs as diagnostic light sources are interesting in respect of their compactness and low cost. As well, it provides sufficient intensity at the desired wavelengths, and any wavelength desired for the diagnostics. The main advantage for the present application of APDs as detectors, instead of a spectrometer used in the previous generation of the system [3], is the short integration time. This makes it possible to correctly subtract any ambient background light in a noise-free manner.

The combined use of reflectance and fluorescence, using different wavelength of interest, optimizes the diagnostic capabilities. The UV light excitation source provides information about tissue autofluorescence properties. The other light sources are employed to compensate for any variations of optical properties of the examined tissue. The use of multiple detection wavelengths in parallel allows to also compensate for any small fluctuations in the LED output by forming dimensionless ratios of detection signals. The violet light is also utilized to induce PpIX fluorophore. Accurate extraction of intrinsic fluorescence could potentially provide better diagnostic accuracy.

The linearity study conducted demonstrates that very low fluorescence signal can be detected in the presence of strong ambient light with the developed system. The ambient light suppression, as a main challenge in previous study, is successfully achieved for improved clinical applicability. Multivariate analysis of the signals has proved a great potential in separating the contributions to the signal from fluorescence, absorption and scattering in a serious of tissue phantom measurements.

The temperature dependency of the internal gain of APDs is

an inherent feature of the APD, is considered as a main source of error. Calibration for the temperature variation has been accomplished by mounting thermistor on each APD in order to monitoring the temperature variation on APDs, and deriving appropriate correction coefficient. This work is still in progress, however it has shown promise in increasing the correlations of the evaluated signal with the PpIX concentration. Future progress in this area will be performed before the next clinical study is conducted. Additional reference measurement before and after each clinical measurement has performed to utilize as a further calibration factor related to other sensitivity variations in the signal. This will be continued also in the future clinical measurements, while the variations corrected for by these extra measurements are expected to be minuscule.

The clinical trials on skin tumors were performed in order to test the instrument and its performance. While the data are promising, future work will focus on improving the system performance and preparing the setup to carry out real-time measurement in collaboration with Linköping University for ALA-guided brain tumor resections.

Acknowledgements

Foremost, I would particularly like to express my sincere gratitude to my supervisor, Prof. Stefan Andersson-Engels for the continues guidance and support through of my Master study and patiently proof-reading my thesis. His mentorship was of great importance in providing a very nice training experience consistent with my future career goals. Moreover, I would like to give gratitude to Dr. Johan Axelsson who has been a valuable source of help and advice. I have learned many things from him. I would also like to thank Haiyan Xie for her encouragement and insightful comments.

In addition, a thank you to Zhiyuan Xie, who helped me in stages of incipience and her collaboration throughout the entire period of the project. I take this opportunity to express the deepest appreciation to the people who have been instrumental in the successful completion of this project. I am grateful to Dr. Dmitry Khoptyar for his insightful discussion and suggestion. I know that I could always ask him for advice and opinion. I also thank people who weren't part of project but helped me out, including Alfi Shaharin, Sören Johansson, Nina Reistad and all Biophotonic's group members. I have to thanks to Dr. Niels Bendsoe, who has provided us the possibility to complete the clinical measurements in this report.

I am very much indebted to my family, my husband, for their unflagging love and support throughout my life. I would like to thank my friends and all people who have helped and inspired me during my Diploma study.

References

1. Jeffrey N Bruce and Benjamin Kennedy. Glioblastoma Multiforme. pages 1–41, 2009.

2. Martin Hefti, H Maximilian Mehdorn, Ina Albert, and Lutz Dörner. Fluorescence-Guided Surgery for Malignant Glioma : A Review on Aminolevulinic Acid Induced Protoporphyrin IX Photodynamic Diagnostic in Brain Tumors. pages 3–7, 2010.

3. Neda Haj-Hosseini, Johan Richter, Stefan Andersson-Engels, and Karin Wårdell. Optical touch pointer for fluorescence guided glioblastoma resection using 5-aminolevulinic acid. *Lasers in Surgery and Medicine*, 42(1):9–14, 2010.

4. Seattle Cancer Care Alliance. http://www.seattlecca.org/.

5. Available:. http://www.studyblue.com/.

6. Thomas M Kandel, Eric R.; Schwartz, James H.; Jessell. *Principles of Neural Science*. Fourth edition, 2000.

7. Wieslaw L Nowinski. *Biomechanics of the Brain*. Biological and Medical Physics, Biomedical Engineering. Springer New York, New York, NY, 2011.

8. Kristjan R Jessen. Glial cells. *The international journal of biochemistry & cell biology*, 36(10):1861–7, October 2004.

9. David N Louis, Hiroko Ohgaki, Otmar D Wiestler, Webster K Cavenee, Peter C Burger, Anne Jouvet, Bernd W Scheithauer, and Paul Kleihues. The 2007 WHO Classifcation of Tumours of the Central Nervous System. pages 97–109, 2007.

10. Therese A Dolecek, Jennifer M Propp, Nancy E Stroup, and Carol Kruchko. CBTRUS statistical report: primary brain and central nervous system tumors diagnosed in the United States in 2005-2009. *Neuro-oncology*, 14 Suppl 5:v1—-49, November 2012.

11. M Gupta, a. Djalilvand, and D J Brat. Clarifying the Diffuse Gliomas: An Update on the Morphologic Features and Markers That Discriminate Oligodendroglioma From Astrocytoma. *American Journal of Clinical Pathology*, 124(5):755–768, November 2005.

12. Garth M Turner, Jordana F Goren, and Michael L Gruber. Glioblastoma Multiforme: Multidisciplinary Care and Advances in Therapy. (June), 2008.

13. E C Holland. Glioblastoma multiforme: the terminator. *Proceedings of the National Academy of Sciences of the United States of America*, 97(12):6242–4, June 2000.

14. Walter Stummer, Hanns-Jürgen Reulen, Thomas Meinel, Uwe Pichlmeier, Wiebke Schumacher, Jörg-Christian Tonn, Veit Rohde, Falk Oppel, Bernd Turowski, Christian Woiciechowsky, Kea Franz, and Torsten Pietsch. Extent of resection and survival in glioblastoma multiforme: identification of and adjustment for bias. *Neurosurgery*, 64(3):564–576; discussion 564–576, 2008.

15. C Matula, K Roessler, E Schindler, and K Heimberger. Case study : Palliative resection of a glioblastoma using intra-operative CT-guided navigation. 42(1):44–48, 1998.

16. Phiroz E Tarapore, Edward F Chang, and Mitchel S Berger. Surgical Imaging Intra-operative Imaging Techniques During Surgical Management of Gliomas. pages 163–168, 2011.

17. R. F. Keep A. Novotny, J. Xiang, W. Stummer, N. S. Teuscher, D. E. Smith. Mechanisms of 5-Aminolevulinic Acid Uptake at the Choroid Plexus. *Journal of Neurochemistry*, 2000.

18. P Hinnen, F W de Rooij, M L van Velthuysen, a Edixhoven, R van Hillegersberg, H W Tilanus, J H Wilson, and P D Siersema. Biochemical basis of 5-aminolaevulinic acid-induced protoporphyrin IX accumulation: a study in patients with (pre)malignant lesions of the oesophagus. *British journal of cancer*, 78(5):679–82, September 1998.

19. Martin Hefti, Fabian Holenstein, Ina Albert, Herbert Looser, and Vera Luginbuehl. Susceptibility to 5-aminolevulinic acid based photodynamic therapy in WHO I meningioma cells corresponds to ferrochelatase activity. *Photochemistry and photobiology*, 87(1):235–41, 2011.

20. Daniel L Stout and Frederick F Becker. Heme Synthesis in Normal Mouse Liver and Mouse Liver Tumors Heme Synthesis in Normal Mouse Liver and Mouse Liver Tumors. pages 2337–2340, 1990.

21. Erik Alerstam. *Optical spectroscopy of turbid media : time-domain measurements and accelerated Monte Carlo modelling*. Phd thesis, Lund University, 2011.

22. Chedekel M Kollias N, Sayer R, Zeise L. Photoprotection by melanin. *J Photochem Photobiol B*, 1991.

23. P. Riederer H. Fedorow, F. Tribl, G. Halliday, A. Gerlach, K. L., and Double. Neuromelanin in human dopamine neurons: Comparison with peripheral melanins and relevance to Parkinsons disease. pages 109–124, 2005.

24. Oana C Marina, Claire K Sanders, and Judith R Mourant. Correlating light scattering with internal cellular structures. *Biomedical optics express*, 3(2):296–312, February 2012.

25. Alois K Popp, Megan T Valentine, Peter D Kaplan, and David a Weitz. Microscopic origin of light scattering in tissue. *Applied optics*, 42(16):2871–80, June 2003.

26. G. A. Wagnieres, W. M. Star and B. C. Wilson. "In Vivo Fluorescence Spectroscopy and Imaging for Oncological Applications,". *Photochemistry and Photobiology*, 68:603–632, 1998.

27. Yicong Wua and Peng Xia. Fluorescence spectroscopy of biological tissue : single- and two-photon excitation. *SPIE Proceedings*, 5323:0–4, 2004.

28. N Ramanujam. Fluorescence spectroscopy of neoplastic and non-neoplastic tissues. *Neoplasia (New York, N.Y.)*, 2(1-2):89–117, 2000.

29. B Y Michael R Duchen and T J Biscoe. Mitochondrial function in type i cells isolated from rabbit arterial. *Journal of physiology*, pages 13–31, 1992.

30. H Andersson, T Baechi, M Hoechl, and C Richter. Autofluorescence of living cells. *Journal of microscopy*, 191(Pt 1):1–7, July 1998.

31. Malgorzata Wachowska, Angelika Muchowicz, Malgorzata Firczuk, Magdalena Gabrysiak, Magdalena Winiarska, Malgorzata Wanczyk, Kamil Bojarczuk, and Jakub Golab. Aminolevulinic Acid (ALA) as a Prodrug in Photodynamic Therapy of Cancer. *Molecules*, 16(12):4140–4164, May 2011.

32. V. W. Stummer, H.-J. Reulen, T. Meinel, U. Pichlmeier, W. Schumacher, J.-C. Tonn, Rohde, F. Oppel, B. Turowski, C. Woiciechowsky, K. Franz, and T. Pietsch. Extent of resection and survival in glioblastoma multiforme: Identification of and adjustment for bias. *Neurosurgery-online*, 62:564–576, 2008.

33. Eds W. A. Hall, C. Nimsky, and C. L. Truwit. Intraoperative MRI-Guided Neurposurgery. *Thieme Medical Publishers Inc*, 2010.

34. Walter Stummer, Uwe Pichlmeier, Thomas Meinel, Otmar Dieter Wiestler, Friedhelm Zanella, and Hans-Jürgen Reulen. Fluorescence-guided surgery with 5-aminolevulinic acid for resection of malignant glioma: a randomised controlled multicentre phase III trial. *The Lancet Oncology*, 7(5):392–401, May 2006.

35. WT Mason. *Fluorescent and Luminescent Probes for Biological Activity: A Practical Guide to Technology for Quantitative Real-Time Analysis.* Second edition.

36. Oregon Medical Laser Centre. http://www.omlc.ogi.edu.

37. Ann Johansson, Gesa Palte, Oliver Schnell, Jörg-Christian Tonn, Jochen Herms, and Herbert Stepp. 5-Aminolevulinic acid-induced protoporphyrin IX levels in tissue of human malignant brain tumors. *Photochemistry and photobiology*, 86(6):1373–8, 2010.